*17th World Conference on Earthquake Engineering, 17WCEE*
*Sendai, Japan - September 13th to 18th 2020*

# EFFECTS OF SPATIAL RESOLUTION IN PROBABILISTIC TSUNAMI INUNDATION HAZARD ASSESSMENT

R. Saito[(1)], Y. Murata[(2)] , T. Shibuki[(3)], T. Kito[(4)], K. Oshima[(5)], M. Korenaga[(6)], Y. Abe[(7)], H. Nakamura[(8)], K. Hirata[(9)], H. Fujiwara[(10)]

[(1)] *Engineer, Kokusai Kogyo Co.,Ltd.(KKC), ryu_saito@kk-grp.jp*
[(2)] *Engineer, Kokusai Kogyo Co.,Ltd.(KKC), yasuhiro_murata@kk-grp.jp*
[(3)] *Engineer, Kokusai Kogyo Co.,Ltd.(KKC), tomoyuki_shibuki@kk-grp.jp*
[(4)] *Expert engineer, OYO Corporation, kitou-tadashi@oyonet.oyo.co.jp*
[(5)] *Engineer, OYO Corporation, oshima-kenshi@oyonet.oyo.co.jp*
[(6)] *Engineer, ITOCHU Techno-Solutions Corporation(CTC), mariko.korenaga@ctc-g.co.jp*
[(7)] *Engineer, ITOCHU Techno-Solutions Corporation(CTC), yuta.abe.150@ctc-g.co.jp*
[(8)] *Deputy Manager, National Research Institute for Earth Science and Disaster Resilience(NIED), manta@bosai.go.jp*
[(9)] *Principal Chief Researcher, National Research Institute for Earth Science and Disaster Resilience(NIED), khirata@bosai.go.jp*
[(10)] *Manager, National Research Institute for Earth Science and Disaster Resilience(NIED), fujiwara@bosai.go.jp*

## Abstract

Aimed at contributing to risk assessment and disaster response in coastal areas of Japan, it is necessary to perform a tsunami run-up calculation and evaluate probabilistic tsunami inundation hazards in urban coasts, using huge number of seismic source models built for probabilistic tsunami hazard assessment of Japanese coasts. We therefore performed tsunami run-up calculations to assess stochastic hazards in a moderately urban area on the Pacific coast, using 4,000 seismic source models set in the expected focal zone of Nankai Trough megathrust. The regional characteristics of probabilistic flooding information were discussed from the aspects of topographic resolution and levee defense effect.

The probabilistic tsunami inundation hazard assessment in coastal regions can be quantified using much inundation area and depth information, resulted from tsunami run-up simulations with many seismic source models. One of efforts to obtain reliable and detailed the probabilistic inundation information depends on computing cost such as spatio-temporal resolution of tsunami run-up simulations. It is important to require accurate fine-resolution bathymetry data to evaluate the probabilistic tsunami inundation hazards in areas such as important facilities and densely inhabited district in detail. With using the finer surface model above, we can quantify a different of the probabilistic tsunami inundation hazards between a potential inundation hazard without any structures and an inundation hazard protected with structures, which will be applicable for a performance of levees.

In this study, to investigate effects of differences in spatial resolution and structure conditions in run-up tsunami simulation on the inundation information, we applied spatial resolutions of coarse (50 meters) and fine (10 meters) with conditions of structures and no structures. Then, we compared the simulation-derived inundation information of 10 m with that of 50 m to investigate effects of spatial resolution in run-up tsunami simulation on probabilistic tsunami inundation hazard assessment. An advantage of coarse spatial resolution is to reduce computing cost constrained by a tsunami run-up simulation. In the coarse case, it is implemented as a surface model at 50 m grid size of minimum along coastal regions, however, which is not enough resolution to form an inhomogeneity of terrain topography and built structures which include disaster prevention facilities and levees, seawalls in finer.

Aggregating the results, the tsunami run-up simulations using the many types of the Earthquake scenarios captured a trend and a correlation between the inundation depths of the fine and coarse grid depending on tsunami heights and the structure conditions. We found that the inundation area of the coarse grid is larger than the fine and also the larger the tsunami heights are, the broader the difference between inundation areas of both the resolutions become. Similar trends are obtained for a horizontal distribution of the probabilistic tsunami inundation hazard for the coasts that is described by the hazard curves at every grid points on their run-up areas. Regionality of a performance of levees and potential inundation hazards in the absence of structures were also quantified.

*Keywords: Run-up tsunami simulation; Tsunami inundation; Probabilistic tsunami hazard assessment (PTHA)*




## 1. Introduction

A probabilistic tsunami hazard assessment is being undertaken for all possible tsunami events that will cause major disasters on the Japanese coast [1][2][3]. It assesses the height of the tsunami near the shoreline as a hazard, but by using the same calculation set, we also try to calculate the hazard information of the inundation depth due to the tsunami going up to land.

Probabilistic tsunami hazard assessment (PTHA) of the inundation area is performed using the inundation depth obtained by performing the tsunami propagation run-up calculation with all possible seismic sources and the recurrence rates assigned to each model. The PTHA provides tsunami inundation hazard curves and probabilistic inundation depth maps that share information on the potential for large losses so that companies can prepare for the financial impact.

However, when evaluating the entire coastal area in detail, the calculation cost becomes very high due to the high resolution of the computational grid by refinement and the increase in the number of hazard curves calculated at each evaluation point in the entire area. For this reason, implementing PTHA in coastal areas throughout Japan often practices selecting resources to a feasible number and saving the computational resources by reducing the spatial resolution. Coarse spatial resolution may have significantly different inundation prediction results due to the effect of smoothing fine topography including rugged terrain and the inability to adequately represent protective facilities.

In this study, we focus on the coarse resolution of the spatial resolution of the surface model and the structural conditions in the tsunami run-up calculation using the 4,000 source fault models that generate various tsunami heights for PTHA. We investigate how different resolutions affect the flooded area and PTHA of the inundation area.

## 2. Methodology

### 2.1. Inundation Area to Evaluate

As a test, inundation area to be evaluated is around Wakayama city on the coast of Japan (Fig. 1), with a population of hundreds of thousands. Since Wakayama city is a coastal plain located in the middle of the source area of the Nankai Trough, various tsunamis hit the coast from the east and west sides of the source area. Therefore, we can experiment with various types of tsunami heights and wave directions.

### 2.2. Earthquake Sources Models

We use about 4,000 source models of the Nankai Trough compiled in the previous study [3][4][5], which are created as a set of Characterized Earthquake Fault Models (CEFMs) for all the possible earthquakes. This set of CEFMs has an earthquake magnitude from Mw 7.0 to 9.2.

### 2.3. Surface Models for the PTHA of the Inundation Area

In this study, to investigate effects of differences in spatial resolution and structure conditions in run-up tsunami simulation on the inundation information, we applied spatial resolutions of coarse (50 meters) and fine (10 meters) with conditions of levees and no levees. The B50 column shown in Table 1 indicates a resolution of 50 m, and the other A10, B10, and C10 represent 10 m.

Source data for these terrain models is the same. However, as described above, for the two types of surface models with different resolutions (10 m and 50 m) and the model with a 10 m grid, three types of surface models were created: with levee (A10), smoothing with triangulated irregular network (B10), and no levee (C10). The surface model B50 is smoothed by the triangulated irregular network like B10. So, the B10 and B50 differ only in resolution, but the structure conditions are the same. Table 1 shows the schematic of



 



the surface models. The smoothing can be considered as a situation in which the levee is destroyed or subsided by ground subsidence, seismic motion, liquefaction, or remains halfway. The terrain model C10 has no levees, implying potential hazard of the land or the worst scenario.

In the surface model B50, levee, rivers, and small hills smaller than the 50 m grid are not correctly reflected in the surface model by the smoothing. If the grid size is large, the triangulated irregular network rounds the surface model and loses surface refinement. As shown in Table 1, the top of the structure also tends to be lower than the actual one, and is not represented by the correct height. In the case of surface

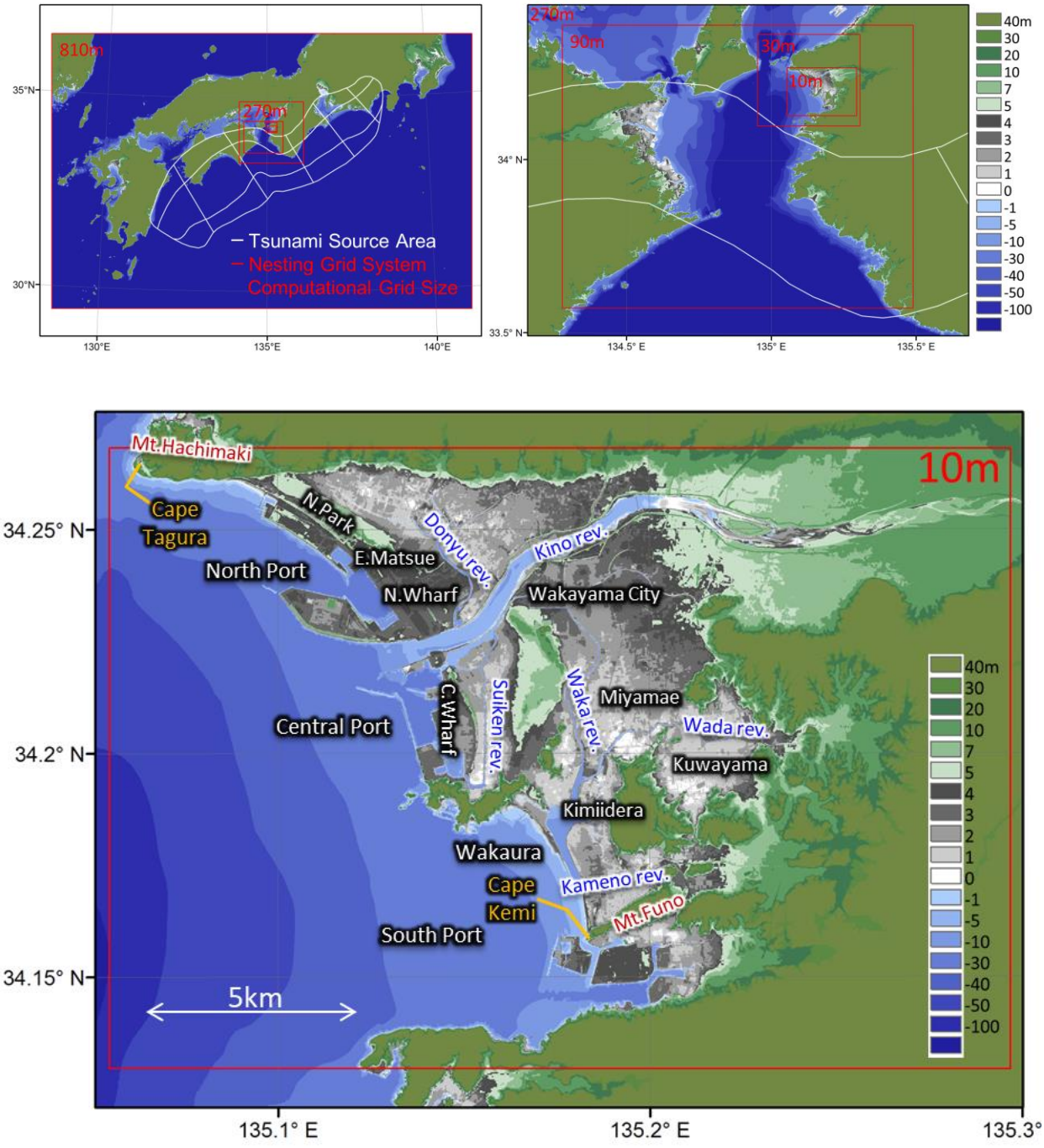


Fig. 1 – Geometry and nesting of the computational grids used to perform the tsunami simulations.



 



model B10, terrain undulations and levees are reflected in B10 at a resolution of 10 m. Therefore, undulations and levee's top are more detailed than the B50, with higher peaks and deeper troughs. For both B50 and B10 of the surface model, the levee top is not correctly reflected. Therefore, the inundation depth distribution is considered to be overestimated when there is an unbreakable levee, and conversely it is considered to be underestimated when there is no levee.

In the surface model A10, the elevation of the grid corresponding to levee and river was corrected to top and bottom obtained from observational data, respectively, based on the source data. In the surface model C10, the river is corrected to the bottom as in the A10, but the top of the levee is shaved to make the ground level.

Tsunami simulation are performed using these surface models to evaluate the inundation depth in the coastal area of Wakayama city. By comparing the inundation depth of the surface model B10 with the inundation depth of the surface model B50, it is possible to know the effect on the inundation depth due to the difference in resolution including the smoothing effect. The difference in the effect of levee's protection on the inundation depth can be found by comparing the inundation depth of the surface model A10 with that of the surface model C10.

Table 1 – Calculation conditions for the inundation simulations.

| | B50 | A10 | B10 | C10 |
|---|---|---|---|---|
| Condition | Smoothed Surface | With levee | Smoothed Surface | No levee |
| Equation | The non-linear long-wave theory | | | |
| Numerical Scheme | The staggered-leapfrog finite differencing | | | |
| Source | Approximately 4,000 fault models from 7.0 to 9.2 Mw along the Nankai Trough[3][4][5] | | | |
| Nesting Grid | 1350 m, 450 m, 150 m, 50 m | 810 m, 270 m, 90 m, 30 m, 10 m | | |
| Elapsed Time | 12 hours | | | |
| Initial Tsunami Distribution | Filtered[6] total vertical and horizontal displacements of seabed deformation[7][8] | | | |
| Tide Level | Tokyo Peil (T.P.) | | | |
| Schematic of Topography and Structure (Levee) Model | 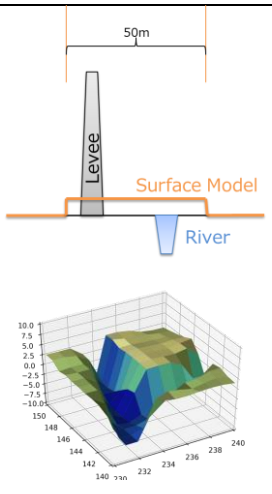 | 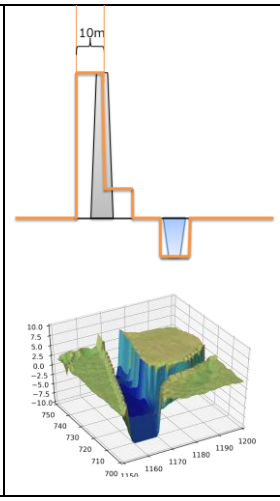 | 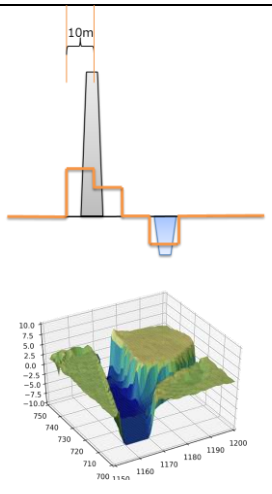 | 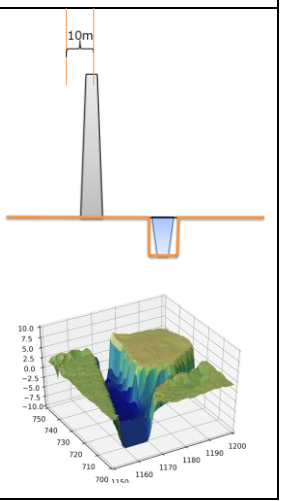 |



 



### 2.4. Tsunami Simulation

Table 1 shows the simulation conditions. We used the staggered leapfrog finite-difference method with the non-linear long-wave theory, which is the most common technique for the simulations of tsunami propagation. The elapsed time was set to 12 hours.

The initial sea surface of the tsunami is calculated based on a study on the total vertical and horizontal displacement of seabed deformation [7][8], and is filtered by the method of Kajiura [6]. The water level standard corresponds to mean sea level of Tokyo Bay (Tokyo Peil, T.P.).

The tsunami simulation adopted the nesting method for streamlined calculations to implement than the size of mesh in the coastal area is expected to be huge more smaller, on the other hand, the size of mesh of the open sea more bigger. This also can shorten calculation time. Figure 1 shows the created surface model for 10 m resolution. The surface models made with a 50 m grid (A10, B10, and C10) are nested in wide 30 m, 90 m, 270 m, and 810 m grid regions. Similarly, the surface model (B50) is nested in wide 150 m, 450 m and 1350 m grid regions.

The roughness coefficient was set to 0.025 for both water and land. Inundation information is affected by roughness, of course, but in this study, we ignore the effect of roughness and focus on the evaluation of only the effects of levees and topography.

### 2.5. PTHA of Inundation Area

An output of the PTHA of the inundation area is inundation hazard map displaying the exceedance probability that has inundation depth exceeding 3 meters in 30 years. The inundation hazard map is drawn based on hazard curves that are computed for each grid cell on the inundation area. We can derive the hazard curves in terms of inundation depth and their annual recurrence rates set as a “long-time averaged hazard”. The “long-time averaged hazard” shows a tsunami risk occurring once in thousands or tens of thousands by estimating earthquake occurrence probabilities applying a stationary Poisson process [9][10], i.e., the probability that the inundation depth will exceed 3 meters at inundation grid cells in next 30 years.

## 3. Results and Discussion

### 3.1. Inundation Depth

The following shows the results of the tsunami run-up calculations assuming a tsunami caused by an earthquake along the Nankai Trough using about 4,000 CEFMs.

Some examples of calculation results are shown in Fig. 2. The upper row shows the calculation results with the maximum inundation area for the ground surface models B50, A10, B10, and C10, and the lower row shows the calculation results with the maximum. In Fig. 3, the number of inundations counted for each grid is displayed on the map as the inundation rate (normalized frequency), using the inundation calculation results of selected 1,300 CEFMs that result in a coastal tsunami height exceeding 2 m. The coastal tsunami height is the average of the maximum tsunami height at all the computational grids near the shoreline from Cape Tagura to Cape Kemi. Therefore, it reflects the frequency of large-scale inundation.

From Fig. 2 showing the inundation depth distribution map, it can be seen that the inundation depth and the inundation area decrease in the order of the surface models B50, C10, B10, and A10. This is because, as shown in the schematic diagram in Table 1, if the grid size is large, the height of the levee and the undulations of the terrain are smoothed, and the factors that obstruct the run-up of the tsunami are reduced, making it easier to flood.

According to Fig. 3, the inundation rate is in the same order as the trend of inundation information shown in Fig. 2. The area around the Waka and Kameno rivers is more easily flooded than the area around the Kino river. This is because the top of the levee is more than 5 m along the coast of the North Port area



 



and the Central Port area and along the Kino river, whereas it is mainly less than 5 m along the Wakaura coast, the Wada and Kameno rivers. On the other hand, comparing the results of the inundation rates between the surface models B50 and B10, the difference in the inundation area is particularly noticeable around East Matsue along the Donyu River and around Kuwayama along the Wada River. The inundation of B50 has reached a wide area. This is probably because the surface model B50 has a lower resolution than the B10 and the terrain is almost flat, which makes it easier to flood.

Comparing the surface models B10 and C10, it was found that C10 excluding levees were more prone to flooding than B10 around the Kino River. However, there was no significant difference in the inundation rates around the Waka River and the Kameno River. This is because there is almost no high levees around the rivers, and the low levees are mainly composed of terrain around the rivers. The low levees are smoothed, so B10 is similar to C10. Therefore, it is considered that the inundation area was similar. On the other hand, a large embankment was originally present around the Kino River, and it remained without being removed by the smoothing of B10. It is probable that the remaining embankment hindered run-up, and that B10 was less likely to be flooded than C10 and the inundation area was smaller.

Even in a compact city with a lowland area of less than 10 km$^2$, such as the whole area of Wakayama

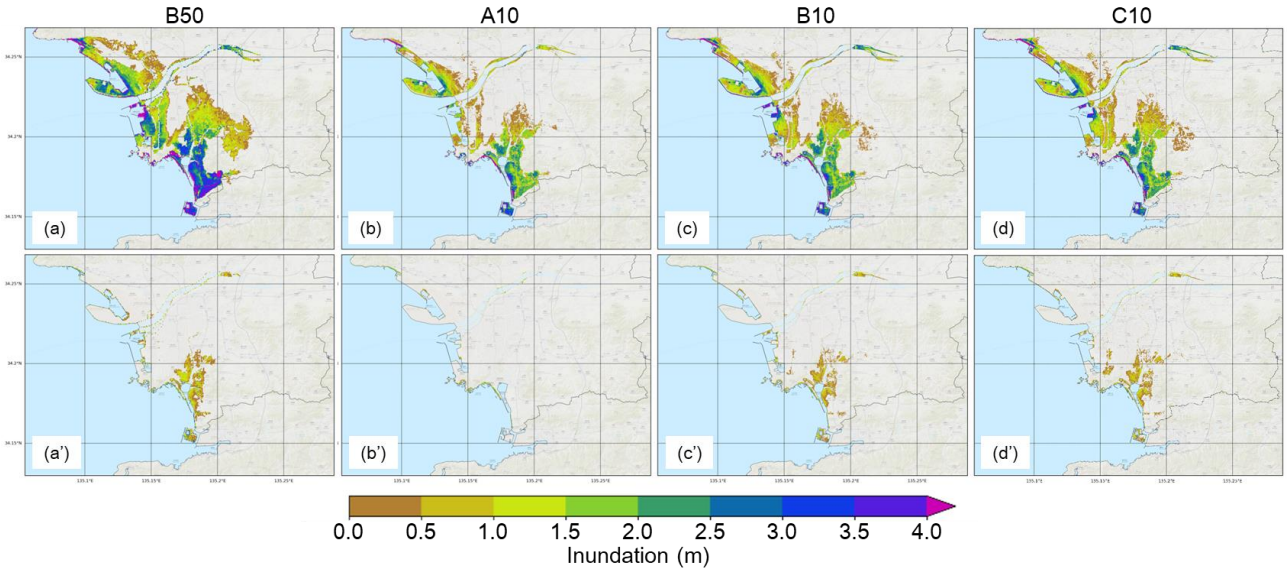


Fig. 2 – Largest inundation area (top panels) and smallest one (bottom panels) among the model-derived maximum inundation depths derived using all sources for each condition shown in Table 1.

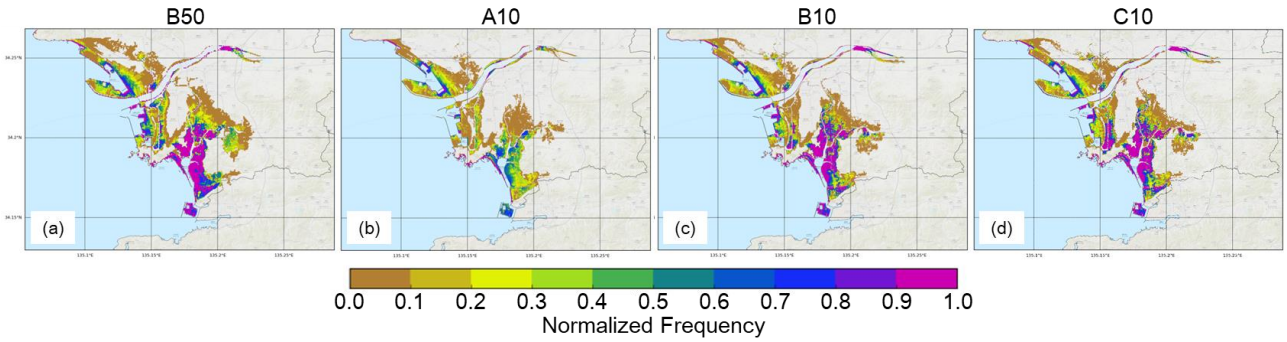


Fig. 3 – Inundation frequency for 1,300 largest events with coastal wave heights greater than 2 m for each condition shown in Table 1.



 



City, the characteristics of inundation distribution differ depending on the levee conditions and river scale.

## 3.2. Inundation Area and Coastal Tsunami Height

Figure 4 shows the correlation between the inundation area and the coastal tsunami height calculated using the 4,000 CEFMs in order to quantify the difference in inundation depth distribution on the surface models B50, A10, B10 and C10. The dots shown in Fig. 4 are the results for each of the 4,000 sources, and the dashed lines are approximations from a linear regression analysis of 4,000 dots. The standard deviation (SD) of the dots with respect to the approximation line is shown in the legend box.

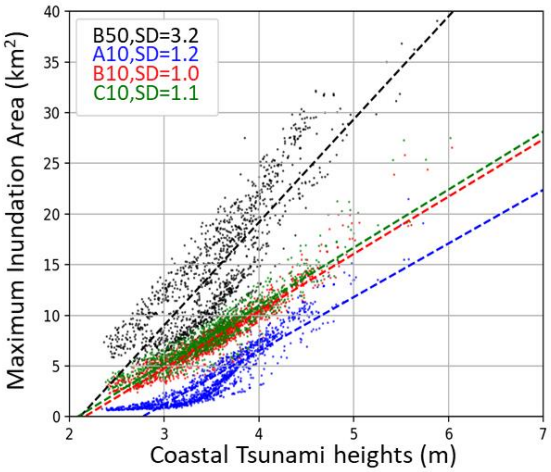


Fig. 4 – Probabilistic tsunami inundation hazard map with inundation depth exceeding 3 m (top panels) and 1 m (bottom panels) obtained using all sources for each condition shown in Table 1.

Regarding the standard deviation SD of the inundation area, results of B50 was larger than B10, A10, and C10, and B10, A10, and C10 were almost the same value. The slope of the fitting line of this correlation was also B50 larger than B10, A10, and C10, and B10, A10, and C10 were almost the same. This indicates that the tsunami run-up of the surface model B50 progresses better than B10, A10, and C10, and the inundation area becomes larger. The previous study [11] also reported that the coarser the resolution, the more likely the inundation range would be overestimated. It can be concluded in this result that the B50 has a coarser resolution than the others, and the inundation area tends to be larger.

In Fig. 4, the slopes of the fitting lines B10, A10, and C10 showed almost the same value. However, the section, that is, the inundation area, was the smallest for the surface model A10, and B10 and C10 were almost the same. The reason that B10 and C10 are almost the same value is because it greatly depends on the inundation rate around the Waka and Kameno rivers (Fig. 3). The water infiltration rates B10 and C10 are both higher than A10, and the water is easily flooded. This feature was reflected in the slope.

## 3.3. Inundation Hazard Map

Figure 5 shows the results of the inundation hazard at eight sites indicated in Fig. 1: (a) Kimiidera, (b) North Port, (c) Wakayama City, (d) North Park, (e) North Wharf, (f) Central Wharf, (g) Kuwayama, and (h) Wakaura. The characteristics of the hazard curves calculated by the surface models B50, A10, B10, and C10 at each of the eight sites are described below.

The hazard curves shown in panels (a), (c), and (h) in Fig. 5 are the exceedance probability in 30 years of the maximum inundation depth calculated on a grid cell in Kimiidera, riverside of Wakayama City, and Wakaura beach, respectively. In these areas, the exceedance probability calculated using the surface model B50 was the largest, and the values calculated using A10, B10, and C10 were almost the same. Therefore, comparing the hazard curves of B50 and B10, the exceedance probability in these regions is affected by spatial resolution refinement. On the other hand, the comparison of A10, B10, and C10 shows that the difference was not affected by the difference in the ground conditions of existence of levees and smoothing. Moreover, because Wakaura beach in the panel (h) is waterside land than is not protected by levees, so the frequency of inundation is the highest compared to the other sites.



 



Panels (b), (d), and (f) in Fig. 5 show the results for North Port, coastal lowlands of North Park, and Central Wharf, respectively. Also in these sites, the surface model B50 had the highest exceedance probability in 30 years as before. However, the exceedance probability of A10 became the smallest. In panel (f), the hazard curve of A10 is not displayed because it is less than $10^{-5}$. The exceedance probabilities of B10 and C10 are almost the same. This means that the exceedance probability depends not only on spatial resolution but also on differences in levee conditions. Since the levees prevent the tsunami run-up, the

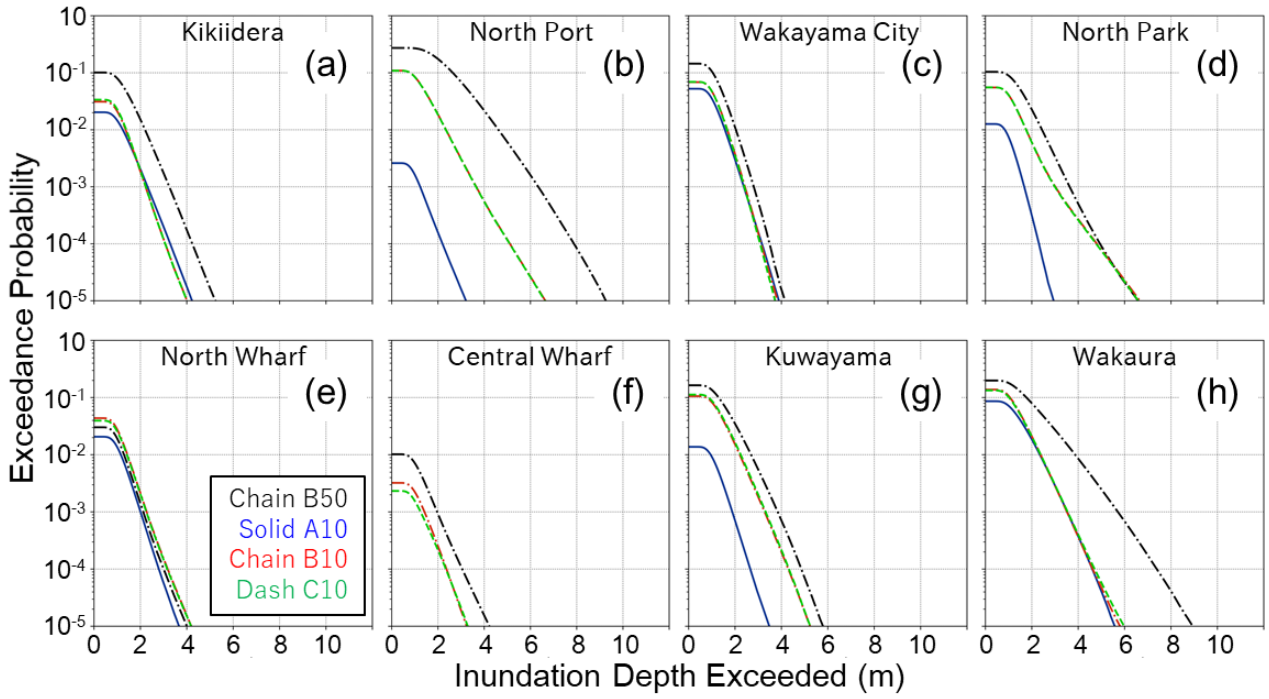


Fig. 5 – Tsunami inundation hazard curve.

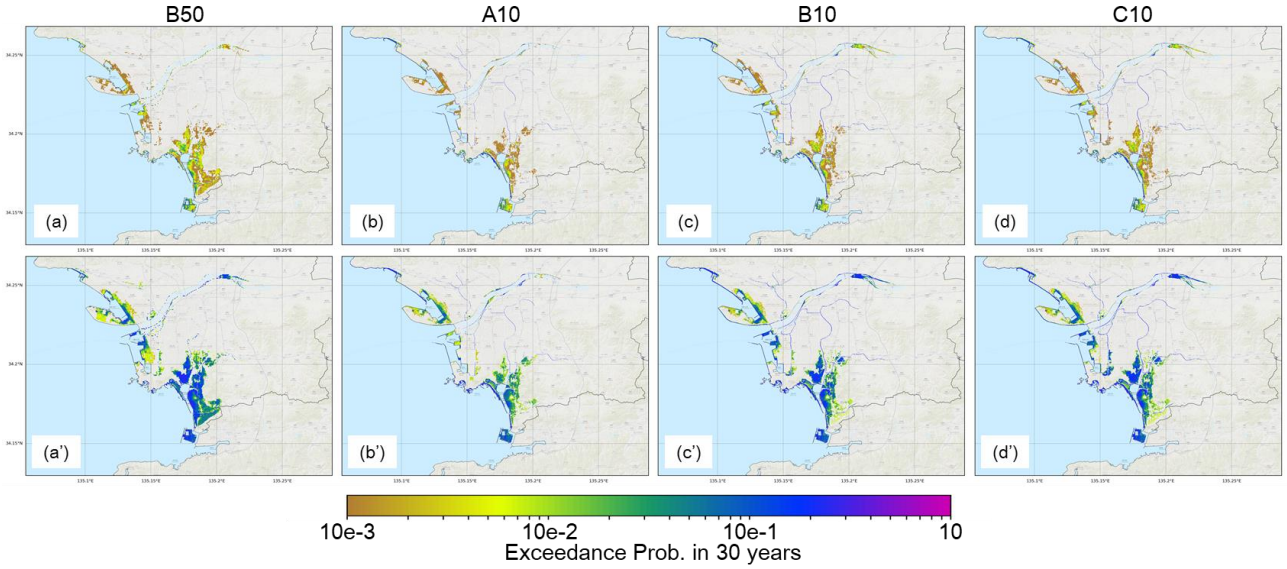


Fig. 6 – Probabilistic tsunami inundation hazard map with inundation depth exceeding 3 m (top panels) and 1 m (bottom panels) obtained using all sources for each condition shown in Table 1.



 



frequency of inundation into the landside area is reduced so that the hazard curve of the A10 is relatively smaller than the other conditions.

Panel (e) in Fig. 5 shows the result for North Wharf. For all of the surface models B50, A10, B10, and C10, the exceedance probabilities in 30 years are almost the same. At this site, the exceedance probability does not change significantly due to differences in spatial resolution and levee conditions. It is the only site where the exceedance probability of B50 is smaller than B10.

Panel (g) in Fig. 5 shows the result for Kuwayama in the inland area. The exceedance probability in 30 years of the surface model B50 is greater than $10^{-4}$, and the exceedance probability of A10, B10, and C10 is less than $10^{-5}$ or not wet, so it is not shown. Since this site is located on the inner land and far from the coast, it is least inundated than other sites. The exceedance probability is greatly affected by differences in spatial resolution. It is considered that the coarser resolution has caused the exceedance probability of B50 to be higher than the other conditions.

Hazard curves on all other flooded grid cells are calculated in the same way as the hazard curves built at each site, and the exceedance probability distribution of the entire tsunami run-up is mapped, as shown in Fig. 6. The upper panels in Fig. 6 are the probabilistic tsunami inundation hazard map with inundation depth exceeding 3 m and lower panels are 1 m. The following features are observed from the results shown in Fig. 6.

In Fig. 6, the distribution patterns of the exceedance probabilities around North Port area, a coastal zone that spans North Park, East Matsue, and North Wharf, are almost the same for all terrain models B50, A10, B10, and C10, both above 1 m and above 3 m. In the Central Port area, which is a lowland zone including the surrounding areas of Central Wharf and the Suiken River, the exceedance probability distribution is larger for the topographic model B50 and smaller for A10. In the South Port area, which is a lowland zone from Kimiidera to Wakaura Beach near the mouth of the Waka River, the map of the exceedance probability of inundation depth exceeding 1 m (upper row in Fig. 6) is the same as the Central Port area described earlier, with the surface model B50 large and A10 small. On the other hand, the exceedance probability distribution of the inundation depth exceeding 3 m (bottom row in Fig. 6) shows that B50 is larger than the others, but A10 has almost the same probability as B10 and C10 without levees. The levees seem to have no effect. This is because in the South Port area, the height of the levee's top is low, so a high tsunami that greatly exceeds the top is likely to hit, and this levee allows the tsunami to run up. Figure 3 also shows that the frequency of large tsunami infestations exceeds 70%. Therefore, it is thought that ultimately the maximum inundation depth is not strongly affected by the presence or absence of levee. In all areas, the exceedance probabilities of the terrain models B10 and C10 had almost the same distribution. This indicates that the difference in ground conditions between B10 (smoothing) and C10 (levee removal) has little effect on the exceedance probability of the inundation depth.

## 4. Conclusion

We performed tsunami run-up calculations to assess stochastic hazards in a moderately urban area, Wakayama City, on the Pacific coast, using 4,000 Characterized Earthquake Fault Models (CEFMs) set in the expected focal zone of Nankai Trough megathrust. Regional features of stochastic tsunami inundation information were discussed in terms of topographic resolution and levee protection effects. To investigate effects of differences in spatial resolution and structure conditions in run-up tsunami simulation on the inundation information, we applied spatial resolutions of coarse (50 meters) and fine (10 meters) with conditions of levees and no levees. Four types of surface models are built: B50 considers damaged levees at 50 m resolution, and A10 with levees, B10 damaged levees, and C10 no levees at 10 m resolution.

In the correlation between the maximum tsunami height of the coast and the inundation area derived from the results of the 4,000 CEFMs (Fig. 4), the slope of the scatter distribution is larger in the surface model B50 than in B10, A10 and C10, and the slope of B10, A10 and C10 is almost the same. In other words, it implies that B50 tends to run up more easily than B10, A10 and C10, and the inundation area tends to be



 



large. The reason why the coarse calculation grid extends the inundation area is because the grid size is large. The lower resolution smoothes topographic ruggedness such as levee, rivers and hills, and reduces the factors that block tsunami run-up. It is thought that the tsunami was easier to run and to reach the inner lands. Therefore, it can be confirmed that the inundation area is larger at 50 m than at 10 m.

As described above, it was found that the inundation frequency tends to be higher for the 50 m grid. It was also found that as the tsunami height along the coast increased, the difference in the inundation area obtained with the 10 m and 50 m grids also increased. As a result, the inundation hazard was larger for the 50 m grid than for the 10 m grid. These suggest that both the "sparse density of spatial resolution" and the "tsunami scale" of the surface model used in the tsunami run-up simulation strongly influence the inundation area and the maximum inundation depth. If you want to use the inundation depth results obtained with the 50 m surface model as municipal inundation hazards, it should be noted that the results include the above-mentioned characteristics.

The difference of the levee condition was investigated for the ground model of 10 m grid size. The scale of the inundation area and the maximum inundation depth when using the topographic model B10 was almost the same as the result when using C10. On the other hand, in the case of the terrain model A10, the area where the tsunami invading is higher than the structure, that is, in the South Port area, the acceleration of the tsunami run-up has the same tendency as when using the terrain model C10 without levees. In other North Port and Central Port areas, levees have reduced tsunami inundation hazards. If the levee is high enough and it does not break at all even in a catastrophe, the effect of preventing the tsunami inundation or delaying the run-up is recognized. As shown in Fig. 5, the effect of levee on flood damage was not only quantified graphically, but also as shown in Fig. 6 by stochastic means. In this way, the inundation area and inundation depth are considered to have regionality because local-specific features such as topography and structural conditions affect tsunami run-up. Therefore, the relationship between inundation depth and coastal tsunami height obtained in Fig. 5 does not perfectly apply to other regions. In particular, in areas such as Tokyo, Nagoya and Osaka where a below-sea-level area spreads, if there is no levee such as the surface model C10, a large amount of water already flows into the land at the start of the calculation, so the correlation plot shown in Fig. 5 will be quite different.

In this study, three types of levee height were set. In order to properly discuss the effects of the levee, it is necessary to add the experimental results of another levee height to Fig. 5 and investigate the relationship between the levee height and the tsunami height in more detail. If a large levee is blindly laid in the city, it will certainly protect the land area completely from tsunami flooding, but it is not realistic in terms of landscape and finances. Perhaps by deepening the quantitative considerations shown in Figs. 5 and 6 in more levee conditions, we can find the best levee height for cost and benefit. This will help provide more specific risk information, such as stochastic assessment of infrastructure facilities, factories, schools, evacuation routes, etc.

## 5. Acknowledgements

This study was done as a part of the research project "Research project on hazard and risk assessment for natural disasters" that is carried out by NIED (National Research Institute for Earth Science and Disaster Resilience). The authors thank that the topographic mesh data released by the "Nankai Trough Massive Earthquake Model Study Group" of the Cabinet Office was used to create our surface model.

## 6. References

[1] Hirata K, et al. (2014, Dec.): Nationwide tsunami hazard assessment project in Japan. *AGU Fall Meeting Abstracts*.

[2] Dohi Y, et al. (2020): Development of Japan Tsunami Hazard Information Station -database of probabilistic tsunami hazard assessment along the Nankai Trough-. 17 WCEE.



 




[3] Kito T, et al. (2020): Probabilistic tsunami hazard assessment along the coast of Japan: fault models and tsunami simulation. 17 WCEE.

[4] Hirata K, et al. (2016, Dec.): Probabilistic tsunami hazard assessment along Nankai Trough (2) a comprehensive assessment including a variety of earthquake source areas other than those that the Earthquake Research Committee, Japanese government (2013) showed. *AGU Fall Meeting Abstracts*.

[5] Toyama N, et al. (2014, May): A set of characterized earthquake fault models for the probabilistic tsunami hazard assessment in Japan. *JpGU Meeting Abstracts*.

[6] Kajiura K (1963): The leading wave of a tsunami. *Bulletin of the Earthquake Research Institute, University of Tokyo*, *41*(3), 535-571.

[7] Tanioka Y, and Satake K (1996): Tsunami generation by horizontal displacement of ocean bottom.*Geophysical Research Letters*, *23*(8), 861-864.

[8] Okada Y (1985): Surface deformation due to shear and tensile faults in a half-space. *Bulletin of the seismological society of America*, *75*(4), 1135-1154.

[9] Hirata K, et al. (2018, Dec.): Integrated probabilistic tsunami hazard assessment against possible tsunamis along the Pacific coast of Honshu and Shikoku islands, Japan. *AGU Fall Meeting Abstracts*.

[10] Abe Y, et al. (2017, May): Integration of probabilistic tsunami hazard assessments along Japan Trench, Nankai Trough and Sagami Trough, *JpGU-AGU Joint Meeting Abstracts*.

[11] Murashima Y, et al. (2008): Study on topographic model using Lidar for tsunami simulation. *Proceedings of ISPRS XXXVII (B8)*, 223-228.



 